JOURNAL OF GEOPHYSICAL RESEARCH: SPACE PHYSICS, VOL. 118, 6500–6510, doi:10.1002/jgra.50584, 2013

Correcting the NOAA/MEPED energetic electron fluxes for detector efficiency and proton contamination

T. Asikainen[1] and K. Mursula[1]

Received 10 April 2013; revised 17 September 2013; accepted 20 September 2013; published 4 October 2013.

[1] The Medium Energy Proton and Electron Detector (MEPED) instruments onboard the NOAA/POES satellites have provided a valuable long-term database of low-altitude energetic particle observations spanning from 1978 to present. Here we study the instrumental problems of the NOAA/MEPED electron detectors and present methods to correct them. It is well known that the MEPED electron detectors are contaminated by protons of certain energy range. Using the recently corrected MEPED proton fluxes, we are now able to reliably remove this contamination. Using a simple simulation model to estimate the response of the MEPED electron detectors to incoming electrons and protons, we show that efficiencies of (Space Environment Monitors) SEM-1 and SEM-2 versions of the detectors have large differences due to different detector designs. This leads to a systematic difference between the SEM-1 and SEM-2 measurements and causes a significant long-term inhomogeneity in measured MEPED electron fluxes. Using the estimated efficiencies, we remove the proton contamination and correct the electron measurements for nonideal detector efficiency. We discuss the entire 34 year time series of MEPED measurements and show that, on an average, the correction affects different energy channels and SEM-1 and SEM-2 instruments differently. Accordingly, the uncorrected electron fluxes and electron spectra are severely distorted by nonideal detector efficiency and proton contamination, and their long-term evolution is misrepresented without the correction. The present correction of the MEPED electron fluxes over the whole interval of NOAA/POES measurements covering several solar cycles is important for long-term studies of, e.g., magnetospheric dynamics, solar activity, ionospheric research, and atmospheric effects of energetic electrons.

Citation: Asikainen, T., and K. Mursula (2013), Correcting the NOAA/MEPED energetic electron fluxes for detector efficiency and proton contamination, *J. Geophys. Res. Space Physics*, *118*, 6500–6510, doi:10.1002/jgra.50584.

1. Introduction

[2] The polar orbiting NOAA/POES satellites have been measuring energetic particles nearly continuously since 1978 with their SEM (Space Environment Monitor) instrument package, which contains the MEPED (Medium Energy Proton and Electron Detector) instrument. This long-running series of measurements presents a unique database for space weather and space climate studies. However, up to recently, the use of MEPED data for long-term studies has been restricted due to several instrumental problems that cause systematic errors and long-term inhomogeneities in the measurements. The proton detectors of the MEPED instrument are plagued by the effects of radiation damage and electronic back detector noise, which lead to erroneous fluxes and artificial long-term trends in the data [*Galand and Evans*, 2000; *McFadden et al.*, 2007]. We have recently conducted a quantitative analysis of the effect of these problems on the MEPED proton detectors, and presented a method to systematically recalibrate the entire set of proton measurements from all NOAA/POES satellites [*Asikainen and Mursula*, 2011; *Asikainen et al.*, 2012].

[3] The MEPED instruments also measure energetic electrons, which have been widely used in, e.g., studies of radiation belts [e.g., *Rodger et al.*, 2010; *Lam et al.*, 2010] and energetic electron effects on atmospheric ionization and ion chemistry [e.g., *Sinnhuber et al.*, 2011; *Andersson et al.*, 2012]. The NOAA/POES electron data have also been used as input for various ionospheric, upper atmospheric, and climate models [e.g., *Codrescu and Fuller-Rowell*, 1997; *Callis*, 2005; *Rozanov et al.*, 2005; *Wissing and Kallenrode*, 2009]. The MEPED electron detectors do not significantly suffer from radiation damage due to detector shielding by a thin metallic foil in front of the detector opening, which prevents the penetration of high fluxes of low energy ions that primarily cause the radiation damage. However, despite this shielding, protons above a few hundred kiloelectron volts can penetrate into the electron detector and contaminate

[1]Department of Physics, Centre of Excellence in Research, University of Oulu, Oulu, Finland.

Corresponding author: T. Asikainen, Department of Physics, Centre of Excellence in Research, University of Oulu, PO Box 3000, Oulu FIN-90014, Finland. (timo.asikainen@oulu.fi)

2169-9380/13/10.1002/jgra.50584

Table 1. Nominal Energy Ranges of Electrons and Contaminating Protons for the Three Integral Energy Channels of the MEPED Electron Detectors

Energy Channel	Nominal Energy Range of Electrons	Nominal Energy Range of Contaminating Protons
E1	>30 keV	∼ 135–1000 keV in SEM-1 210–2700 keV in SEM-2
E2	>100 keV	∼ 225–1000 keV in SEM-1 280–2700 keV in SEM-2
E3	>300 keV	∼ 430–1000 keV in SEM-1 440–2700 keV in SEM-2

the electron measurements. This contamination by energetic protons has been recognized for a long time, but its correction has been very difficult due to lack of reliable proton measurements. Some methods for correcting the proton contamination have been suggested [see, e.g., *Lam et al.*, 2010], but reliable usage of such methods has been restricted to those times when the radiation damage of the proton detectors has not progressed too far (generally 1–2 years after satellite launch). However, since we now know the correct proton spectrum, it is possible to reliably remove the contaminating proton counts from all electron measurements.

[4] Another problem in the MEPED electron detector is its nonideal efficiency for detecting electrons. Recently, *Yando et al.* [2011] used a complex Monte Carlo simulation model to estimate the effective geometric factors of the MEPED proton and electron detectors in the SEM-2 version of the instrument package. (The satellites up to NOAA-14 had the SEM-1 version of the instrument package while starting from NOAA-15 the satellites carry an improved version called SEM-2). Their results showed that the detector efficiency, especially in the lowest of the three MEPED electron energy channels, deviates significantly from ideal. The nonideal efficiency is caused by the shielding that prevents the harmful low energy protons from penetrating into the electron detector, because it also effectively scatters the lowest energy electrons measured by the instrument. Such a deviation from ideal detector response leads to underestimation of the electron fluxes and an erroneous electron energy spectrum. This problem also jeopardizes the long-term homogeneity of the entire series of NOAA/POES electron measurements, because the differences in the electron detector design between SEM-1 and SEM-2 will lead to differences in electron detector efficiencies, which cause systematic differences between the SEM-1 and SEM-2 electron measurements. This detector efficiency problem and its effect on the electron measurements have not yet been consistently studied throughout the whole period of MEPED measurements.

[5] The present paper discusses the problems of the NOAA/MEPED energetic electron measurements and is organized as follows. We begin by briefly reviewing the basic facts of NOAA/POES satellites and MEPED instruments in section 2. In section 3, we describe a Monte Carlo simulation model that allows us to estimate the efficiency of the electron detector for incoming electrons and protons both for SEM-1 and SEM-2 instruments. We will show that due to different detector shielding designs, the SEM-1 and SEM-2 versions of the instrument have significantly different detector efficiencies. In section 4, we present an algorithm to correct the electron measurements by removing the proton contamination and correcting for the detector efficiency. In section 5, we compare the uncorrected and corrected electron fluxes and show that the systematic differences between SEM-1 and SEM-2 fluxes are mainly caused by the different detector efficiencies, and are removed by the presented correction. We also discuss the relative effects of proton decontamination and correction for detector efficiency. The final section of the paper presents our conclusions.

2. NOAA/POES Satellites and MEPED Instrument

[6] The NOAA/POES satellites fly on nearly circular, polar orbits with a nominal altitude of about 850 km and an orbital period of about 102 min. The orbital planes relative to the Sun-Earth line stay relatively constant ("Sun synchronous") although over a period of several years, the orientation of the orbital planes of some satellites drifts significantly [*Asikainen et al.*, 2012]. Energetic electrons in MEPED are measured nominally above 30 keV in three integral energy channels, and energetic protons in nominal energy range from 30 keV upward in six differential energy channels (MEPED in SEM-1 package had only five differential proton channels). The nominal energy ranges of the MEPED electron instrument are shown in Table 1.

[7] Both protons and electrons are measured by two nearly orthogonal telescopes, the 0° and 90° telescopes, with a sampling time of 2 s (the two directions are sampled on alternating seconds). In regions where the particle fluxes are very low, the 2 s sampling time can be too short to obtain meaningful counts. To overcome this, we use in this work 16 s averaged measurements (i.e., average of eight consecutive measurements). In SEM-2 the 0° (local vertical) telescope points roughly away from the Earth along the radial Earth-satellite line (toward $-X$ axis in satellite coordinates) and the 90° (local horizontal) telescope points almost antiparallel to spacecraft velocity vector (toward $+Y$ axis of the satellite coordinate system). To ensure a clear field of view the 0° telescope has been rotated by 9° from $-X$ axis toward the $-Z$ axis and the 90° telescope has been rotated by 9° from $+Y$ toward $-Z$ axis. (However, in METOP-02 the telescopes point directly toward $-X$ and $+Y$ axes respectively). At high latitudes, where the magnetic field lines near the Earth are nearly radial, the 0° telescope measures roughly field-aligned precipitating particles and the 90° telescope measures roughly locally trapped particles. At low latitudes the situation is opposite so that the 90° telescope measures roughly field-aligned particles (either precipitating or upflowing, depending on the direction of satellite motion and the hemisphere) and 0° telescope locally

trapped particles. However, since the field of view of the telescopes is 30°, the actual range of pitch angles that the telescopes measure can be quite large. In SEM-1 the spacecraft coordinate system and detector orientation differ from those of the SEM-2 satellites. The SEM-1 *X* axis points toward the Earth as in SEM-2 but the *Y* axis points along the spacecraft velocity vector and *Z* axis completes the right-handed set. Accordingly, the *Y* and *Z* axes in SEM-1 are opposite to those in SEM-2. In SEM-1 the 0° telescope is pointed precisely along the *–X* axis (no 9° tilt as in SEM-2). The 90° telescope, however, is pointed toward the *–Z* axis from where it has been rotated by 9° toward *–X* axis. Accordingly, the angle between the orientations of the 0° and 90° telescopes is 81° for SEM-1 and 88.6° for SEM-2. The measured count rates (particles/sec) are converted to physical fluxes (particles/cm^2 sr s) by dividing with the geometric factor *G* of the detector. For SEM-1 the nominal geometric factor is $G = 0.0095$ cm^2 sr and for SEM-2 $G = 0.01$ cm^2 sr. (A more detailed description of SEM-1 is given by *Hill et al.* [1985], *Seale and Bushnell* [1987], *Raben et al.* [1995], and of SEM-2 by *Evans and Greer* [2000]).

3. Modeling the Detector Efficiencies

[8] *Seale and Bushnell* [1987] discussed the details of the NOAA/MEPED instruments and presented detector efficiency curves for the TIROS-N (SEM-1) MEPED electron instrument, which were based on electron beam calibrations performed at NASA/GSFC facilities. These curves show that the detector efficiency, especially for the lowest E1 electron channel, is significantly different from an ideal step-like response curve. Similar results for the SEM-2 instrument were recently obtained by *Yando et al.* [2011] who used a comprehensive Monte Carlo simulation based on the GEANT4 particle simulation code to model the response of the proton and electron detectors of SEM-2 MEPED to an omnidirectional and isotropic particle flux. Their results showed that also the SEM-2 electron detector response, especially in the lowest E1 energy channel, deviates significantly from an ideal response and that the ranges of electron and proton energies to which the electron channels are sensitive are not very sharply defined. These results indicate that the MEPED electron measurements should be corrected not only for proton contamination but also for detector efficiency in order to obtain a reliable estimate of electron fluxes and spectra.

[9] Unfortunately, the detector efficiencies presented by *Seale and Bushnell* [1987] and *Yando et al.* [2011] cannot be straightforwardly applied to all MEPED electron detectors. The structure of the TIROS-N (the first SEM-1 satellite) electron instrument differs slightly from the subsequent SEM-1 electron instruments used in the NOAA/POES satellites, and therefore cannot be used to represent the electron detectors in all SEM-1 satellites. On the other hand, the structure of the SEM-2 instrument is also somewhat different from that of the SEM-1 (and TIROS-N) instrument and because of this, the results of *Yando et al.* [2011] can only be applied to SEM-2 instruments. Thus the previously estimated detector efficiencies cannot be used to correct the electron measurements of all SEM-1 and SEM-2 NOAA/POES satellites.

Table 2. Electronic Energy Ranges of the Three MEPED Electron Channels for SEM-1 and SEM-2 [*Yando et al.*, 2011]

Energy Channel	Energy Ranges for SEM-1	Energy Ranges for SEM-2
E1	25.6 keV–1 MeV	25.6 keV–2.5 MeV
E2	98.1 keV–1 MeV	98.1 keV–2.5 MeV
E3	299 keV–1 MeV	299 keV–2.5 MeV

[10] In order to calibrate all MEPED electron detectors uniformly, we have recalculated the SEM-1 and SEM-2 detector efficiencies with the MULASSIS (Multi-Layered Shielding Simulation Software) particle simulation code [*Truscott et al.*, 2003] based on the GEANT4 toolkit. MULASSIS is designed for analyzing penetrating particle fluxes in a 1-D geometry consisting of either planar or spherical layers of different materials. The code allows one to easily define a set of layers of desired material and thickness and the flux, energy spectrum, and species of incoming particles. A key feature of the code is the possibility to obtain in each layer the amount of energy deposited by each incoming particle (i.e, the pulse height spectrum of incoming particles). MULASSIS is available online with a simple graphical user interface in the SPENVIS system (http://www.spenvis.oma.be).

[11] Using MULASSIS simulation, we have modeled the MEPED electron detector as a set of planar layers on top of each other, according to SEM-1 and SEM-2 instrument specifications. (TIROS-N version of the instrument was left out of this analysis because the required instrument construction details were not available). The SEM-1 instrument is modeled with two layers. The detector layer is made of silicon (Si) and is 700 μm thick. On top of the detector is a 0.511 μm thick nickel (Ni) layer whose purpose is to reduce the detector sensitivity to incoming solar radiation and energetic protons. The SEM-2 instrument contains three layers. Similarly to SEM-1, the detector is a 700 μm thick layer of Si, but the front surface of the detector is covered with an aluminum (Al) layer whose thickness is about 7.41 μm [*Evans and Greer*, 2000]. The Al-layer is further covered with a Ni-layer whose thickness is 0.76 μm. In one MULASSIS simulation, a monoenergetic beam of 10^5 incoming particles was launched toward the detector. The angular distribution of the particle beam was defined isotropic within ±15° relative to the detector normal in accordance with the 30° field-of-view of the detector. The relative number of particles triggering an event in each of the instrument energy channels (i.e., the detector efficiency) was registered. A particle was defined to trigger an event in one of the three energy channels if the energy deposited in the detector layer is in the electronic energy range for the corresponding energy channel (which are given in Table 2). These energy ranges were obtained from *Yando et al.* [2011] following instrument specifications. Note that the energy thresholds determined from in-flight calibrations of SEM-1 instruments by *Seale and Bushnell* [1987] are the same as in SEM-2 instrument, confirming that the two instruments have the same electronic thresholds. The simulation was performed separately for incoming electrons and protons, and the detector efficiency for each channel was recorded as a function of the energy of incoming electrons and protons. Using 15–20 selected energies (roughly regularly spaced in logarithmic scale) of the incoming particle

beam, a sufficiently accurate representation of the efficiency as a function of energy was obtained.

[12] The electronic channel thresholds are not strictly defined as they are subject to electronic noise in the instrument circuitry. Thus, sometimes, an electron with energy slightly below the nominal threshold may trigger an event and sometimes it requires slightly more energy than the nominal threshold to trigger an event. If the noise level is large enough compared to the threshold energy, the detector efficiency can significantly be influenced. The in-flight calibrations performed routinely on the MEPED electron instruments indicate that the channel threshold energies follow Gaussian distributions with a standard deviation of about 2.5 keV. This noise level is roughly the same in all MEPED instruments of all satellites and stays roughly constant over time (D. Evans, personal communication, 2011). To study the effect of this noise on the detector efficiencies, we repeated the MULASSIS simulations for each energy channel by adding an offset of ±2.5 keV to the nominal channel thresholds. We then computed the averaged efficiency curve as a weighted average of the efficiencies simulated using the nominal (weight = 1), nominal –2.5 keV (weight = $e^{-0.5}$) and nominal +2.5 keV (weight = $e^{-0.5}$) threshold energies. The weights correspond to the probability densities of the Gaussian distribution for the distribution mean and one standard deviation. The efficiency curves obtained as a result of this exercise were very close (difference less than 2%) to the efficiencies obtained by using only the nominal channel threshold energy. This indicates that the electronic noise in the MEPED electron detectors does not significantly affect the detector efficiency and we can neglect it.

[13] In addition to the electronic noise, a dead layer, which typically forms on the surface of a Si-detector below the electronic contacts, may also affect the detector efficiency if it is sufficiently thick. Dead layer is a layer of the Si-detector where electric charge cannot be collected, and thus effectively acts as an additional shielding barrier on top of the detector. Unfortunately, because there is no information on the thickness of the dead layer on MEPED detectors, their effect on the detector efficiency cannot be exactly estimated. However, *Elad et al.* [1973] have studied the dead layer thicknesses on Si-detectors similar to those used in the MEPED instruments, and they showed that in the studied detectors, the dead layer thickness is well below 0.2 μm. Using this as an upper bound estimate for the dead-layer thickness, we ran our MULASSIS simulations by including an additional 0.2 μm Si-layer in front of the detector. The resulting efficiency curves were very close (difference less than 5%) to the curves obtained without the dead layer indicating that the effect of the dead layer on the efficiency is negligibly small.

[14] Figure 1 shows the SEM-1 and SEM-2 detector efficiencies as a function of the energy of incoming electrons for the three electron channels obtained from MULASSIS simulations. The simulated efficiencies were interpolated by a piecewise cubic polynomial as a function of logarithmic energy. One can see that the detector efficiencies in SEM-1 and SEM-2 are significantly different from an ideal step-like efficiency curve. E1 efficiency rises quite slowly as a function of energy and reaches 0.95 only around 120 keV even though the nominal energy threshold is 30 keV. Because of this smoothly rising efficiency curve, it is difficult to define

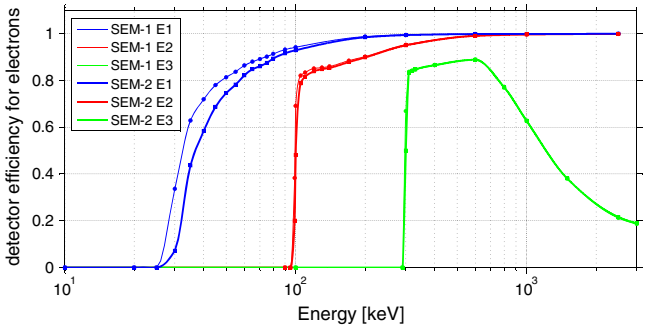

Figure 1. Detector efficiencies as a function of electron energy for the three integral electron channels obtained from the MULASSIS simulation. The circles represent SEM-1 and squares SEM-2 determined from the simulation of selected energies. The curves are piecewise cubic polynomial fits to data points.

a strict energy threshold for the lowest channel. For E2 and E3 channels the efficiency rises quite sharply indicating that the nominal channel thresholds are well defined. However, despite the sharp energy thresholds for E2 and E3 channels, the efficiency does not reach 1.0 immediately after the threshold. For E2 channel the efficiency reaches the value of 0.85 at the threshold, beyond which it slowly rises further, reaching the value of 0.95 at 290 keV.

[15] For E3 channel the efficiency curve differs significantly from the ideal. Similarly to E2 efficiency, the E3 efficiency reaches the value of 0.85 at the threshold, and rises slowly thereafter. However, the E3 efficiency reaches its maximum value of only 0.89 at about 600 keV decreasing thereafter below 0.2 by 2.5 MeV. Note that, as shown by *Yando et al.* [2011], but not seen in Figure 1, the E3 efficiency rises smoothly again after 3 MeV and reaches close to 1.0 after 6 MeV. This is partly because radiative energy losses of electrons in silicon begin to strongly increase at energies above a few MeV. The efficiencies of E1, E2, and E3 do not drop to zero at the upper limit 2.5 MeV (1 MeV in SEM-1) of the electronic energy range because, when the energy of incoming electrons becomes large enough, they pass through the entire detector depositing only relatively small amounts of energy into the Si-layer, well below the upper limit. Accordingly, there is no upper limit of incoming electron energy for any of the three energy channels. Here we have determined the efficiencies only up to the energy of 2.5 MeV for computational reasons. Neglecting the energies above 2.5 MeV does not significantly affect the results of this work because the fluxes at high energies are typically very low and contribute little to the count rates of the three channels.

[16] Comparing the SEM-1 and SEM-2 efficiencies, one can see differences in E1 channel with the efficiency being significantly higher in SEM-1 than in SEM-2. For example, at the nominal threshold of 30 keV, the SEM-1 efficiency is 0.34 but SEM-2 efficiency is only 0.07. At 40 keV, SEM-1 efficiency is about 0.71 but SEM-2 efficiency is only 0.58. Only above 100 keV do the two E1 efficiencies become essentially the same. The form of the E1 efficiency curves is roughly similar for SEM-1 and SEM-2, but the SEM-2 curve is offset by about 5 keV to higher energies. The E2

efficiencies are also different between SEM-1 and SEM-2, but the differences are limited to a rather narrow energy range around the 100 keV threshold. Exactly at 100 keV, SEM-1 E2 efficiency is 0.69 but SEM-2 efficiency is only 0.48. However, already by 120 keV, the difference between SEM-1 and SEM-2 efficiencies is only about 0.01. For E3 channel the differences are even smaller and limited to even narrower energy range around the 300 keV threshold energy. We note that the overall shapes of the three efficiency curves depicted in Figure 1 resemble the shapes of the detector efficiency curves determined by laboratory experiments for TIROS-N presented by *Seale and Bushnell* [1987] and the curves for SEM-2 electron detector determined by simulation by *Yando et al.* [2011]. This gives support to the fact that the 1-D detector model employed here yields a sufficiently accurate estimate for the detector efficiency.

[17] Let us now discuss the physical reasons for the observed differences in the efficiency curves. The difference between SEM-1 and SEM-2 curves is mainly caused by the shielding Ni foil that is about 49% thicker in SEM-2 than in SEM-1. The additional Al-layer used in SEM-2 does not significantly affect the electron efficiency curves. (This was tested by running the simulation also without the Al-layer). The difference between SEM-1 and SEM-2 arises because electrons are efficiently scattered in the material they pass through. The Rutherford scattering cross section is proportional to the square of the atomic number Z of the material. In Ni ($Z = 28$) the scattering cross section is 4.6 times larger than in Al ($Z = 13$) and 4 times larger than in Si ($Z = 14$) due to this factor. The thicker Ni foil in SEM-2 scatters electrons off more efficiently and leads to smaller detector efficiencies. The scattering cross section is also inversely proportional to the square of electron energy. This is why the difference between SEM-1 and SEM-2 efficiencies is largest at low energies and decreases with energy. The reason why the E1 efficiency curves rise so slowly with energy is also because of electrons at energies below 100 keV are efficiently scattered off in Ni. As the energy of incoming electrons increases, the probability of scattering decreases, the electrons can more typically enter the Si detector, when the detector efficiency increases.

[18] Figure 2 shows the SEM-1 and SEM-2 detector efficiencies for the three electron channels in case of incoming protons. The interpolated efficiency curves were computed in the same way as described above for electrons. The ranges of proton energies to which the channels are sensitive are, especially for the E3 channel, quite close to those documented earlier (see Table 1). The nominal energy thresholds of contaminating protons for SEM-1 E1, E2, and E3 are 135 keV, 225 keV, and 430 keV. For E1 and E2 channels, these values correspond roughly to the energies where the determined efficiencies exceed 0.5. For E3 channel, the efficiency exceeds 0.5 at about 395 keV energy, and even reaches the full efficiency slightly below the nominal threshold. Especially in E1 (and less in E2) channel, the detector efficiency deviates from an ideal response at the lower energies. SEM-1 E1 efficiency starts to increase already at 70 keV but reaches 1.0 only at about 200 keV. SEM-1 E2 efficiency begins to increase already at 100 keV, has a slow rise to about 0.1 at 190 keV and then a fast rise close to 1.0 between 200 and 250 keV. For SEM-2 channels the shapes of the efficiency curves are quite similar to SEM-1 but offset in energy.

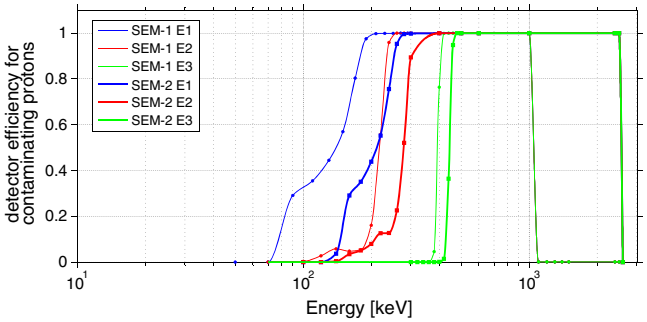

Figure 2. The same as Figure 1 for incoming protons.

The nominal energy thresholds of protons for SEM-2 E1, E2, and E3 channels are 210 keV, 280 keV, and 440 keV (see Table 1). These values correspond very closely to the energies where the efficiency exceeds 0.5. The differences between SEM-1 and SEM-2 efficiencies for protons are also mainly due to the different thickness of the Ni foil shielding the instrument. The upper cutoff in the efficiencies is produced by the upper electronic channel threshold set at 1 MeV in SEM-1 and at 2.5 MeV in SEM-2. Protons above 1 MeV lose relatively little energy as they pass through the Ni foil, while in the Si detector, they lose most of their energy, which is why the upper electronic thresholds closely correspond to the effective thresholds for the incoming proton energy.

4. Correcting the Electron Measurements

[19] The detector efficiencies presented above show that the electron detectors are sensitive to both electrons and protons, that the detector efficiency is significantly different from an ideal step-like response, and that significant differences exist between SEM-1 and SEM-2 detectors mainly due to the different thickness of the shielding Ni foil. To obtain a reliable estimate of the electron fluxes in the three channels so that SEM-1 and SEM-2 fluxes are commensurate, the observations need to be corrected on the basis of the detector efficiency curves. The correction is divided into two parts: removing proton contamination and normalizing the decontaminated electron fluxes by the calculated detector efficiencies.

4.1. Removing the Proton Contamination

[20] Let us begin with a few definitions. We denote the true (initially unknown) differential spectrum of electrons by $f_e(E)$ and the corresponding integral spectrum by

$$F_e(E) = \int_E^\infty f_e(E)\mathrm{d}E. \tag{1}$$

In discrete form, the integral spectrum is

$$F_e(E_i, E_{\max}) = \sum_{E_j=E_i}^{E_{\max}} f_e(E_j)\Delta E, \tag{2}$$

where $E_{\max}$ is the maximum energy the sum is evaluated to and ΔE is a constant defining the energy resolution of the summation. Similarly, we define the differential $f_p(E)$ and integral $F_p(E)$ spectra for protons. Let j_i ($i = 1, 2, 3$) be the observed flux of particles in the ith energy channel in units of

$cm^{-2}sr^{-1}s^{-1}$. This obviously is a combination of electrons and contaminating protons which can be written with continuous functions as

$$j_i = \int_0^\infty \epsilon_i(E) f_e(E) \mathrm{d}E + \int_0^\infty \rho_i(E) f_p(E) \mathrm{d}E, \quad (3)$$

where the $\epsilon_i(E)$ and $\rho_i(E)$ are the electron and proton detection efficiency functions of the ith energy channel. In discrete form, this equation can be written as

$$j_i = \sum_{E_k=0}^{E_{\max}} \epsilon_i(E_k) f_e(E_k) \Delta E + \sum_{E_k=0}^{E_{\max}} \rho_i(E_k) f_p(E_k) \Delta E. \quad (4)$$

The first term describes the contribution of electrons and the second term the contribution of the contaminating protons to the observed flux in the ith channel. Our goal is to estimate the true electron spectra $f_e(E)$ and $F_e(E)$, and to that end we must first estimate and subtract the contribution by the contaminating protons. We have evaluated the interpolated functions $\rho_i(E)$ depicted in Figure 2 in 1 keV spacing (i.e., ΔE=1 keV) between $E_i = [25, 2500]$ keV, and constructed the proton differential spectrum $f_p(E)$ from the corrected MEPED proton measurements [*Asikainen and Mursula*, 2011; *Asikainen et al.*, 2012]. The latter was obtained by first computing the values of the integral proton spectra $F_p(E)$ (analog of equation (2)) in the four (SEM-1) or five (SEM-2) lowest differential proton energy channels (the highest proton channel is contaminated by relativistic electrons), then fitting a piecewise cubic interpolating polynomial to these values and evaluating this integral spectrum polynomial at the same 1 keV spaced energies as $\rho_i(E)$. The differential proton spectrum is obtained by taking the first difference (numerical derivative) of this integral spectrum. Knowing functions $\rho_i(E)$ and $f_p(E)$, we can evaluate the sum in the second term of equation (4) and remove this contribution of contaminating protons from the observed fluxes j_i.

4.2. Estimating the True Electron Fluxes

[21] The final step in correcting the MEPED electron measurements is to estimate the true electron spectra $f_e(E)$ and $F_e(E)$ and to compute from these the true electron fluxes that would be observed at the nominal energy channels. Let us denote by j_i' the observed flux at the ith channel from which the proton contamination has been removed:

$$j_i' = j_i - \sum_{E_k=0}^{E_{\max}} \rho_i(E_k) f_p(E_k) \Delta E = \sum_{E_k=0}^{E_{\max}} \epsilon_i(E_k) f_e(E_k) \Delta E. \quad (5)$$

We now face an inversion problem with three equations (corresponding to $i = 1, 2, 3$) from which an unknown discretized spectrum $f_e(E)$ should be solved. Since $f_e(E)$ should be known at the same 2476 energies as $\epsilon_i(E)$ (and $\rho_i(E)$ and $f_p(E)$) the problem is highly underdetermined and standard inversion techniques based on, e.g., regularized regression or non-negative least squares, produce poor results. A better approach is to assume a theoretically reasonable a priori form for the true spectrum depending on a few parameters, and then to numerically solve these parameters. Here we model $f_e(E)$ with a piecewise power-law function

$$\begin{aligned} f_e(E) &= BE^{-\gamma_1}, \; E < E_{xo}, \\ f_e(E) &= AE^{-\gamma_2}, \; E \geq E_{xo}, \end{aligned} \quad (6)$$

where A, B, γ_1, and γ_2 are unknown constants, and the crossover energy E_{xo} = 95 keV. We further require that $f_e(E)$ is continuous at E_{xo}, so that $B = AE_{xo}^{\gamma 1 - \gamma 2}$. The crossover energy was fixed to a value of 95 keV for two reasons. First, allowing E_{xo} to be a free parameter would result in an underdetermined problem where unique solutions for the unknown parameters could not be obtained. Second, below 95 keV energy, the SEM-1 and SEM-2 E2 and E3 channel efficiencies are zero, and consequently the flux observed at these channels can be written in terms of only A and γ_2, which simplifies solving of the equations considerably. Note also that representing the spectrum with two power law functions with a crossover point approximately at 100 keV energy corresponds to the energy resolution offered by the three energy channels of the MEPED electron detector. Writing equation (5) for $i = 2$ and $i = 3$ and taking their ratio, we obtain

$$\frac{j_2'}{j_3'} = \frac{\sum_{E_k=0}^{E_{\max}} \epsilon_2(E_k) E_k^{-\gamma_2}}{\sum_{E_k=0}^{E_{\max}} \epsilon_3(E_k) E_k^{-\gamma_2}}, \quad (7)$$

where $E_{\max}$ = 2500 keV. In this equation the left hand side is known from observations (after proton decontamination) and the equation can be numerically solved for γ_2 since $\epsilon_2(E)$ and $\epsilon_3(E)$ functions are known. Once γ_2 is known, we can solve A (and B) from equation (5) written for $i = 2$, so that

$$A = \frac{j_2'}{\sum_{E_k=0}^{E_{\max}} \epsilon_2(E_k) E_k^{-\gamma_2} \Delta E}. \quad (8)$$

Writing equation (5) for $i = 1$ gives

$$j_1' = \sum_{E_k=0}^{E_{xo}} A E_{xo}^{-\gamma_2} \epsilon_1(E_k) \left(\frac{E_k}{E_{xo}} \right)^{-\gamma_1} \Delta E + \sum_{E_k=E_{xo}}^{E_{\max}} A \epsilon_1(E_k) E_k^{-\gamma_2} \Delta E. \quad (9)$$

From this equation we can numerically solve γ_1, which completes our solution for the differential electron spectrum. The final step is to use the solved electron spectrum to compute the fluxes in the nominal energy channels. Integrating the differential spectrum in equation (6) from the channel thresholds (E_1, E_2, and E_3) to the maximum energy of $E_{\max}$ = 2500 keV, we obtain the following formulas for the corrected electron fluxes:

$$\begin{aligned} j_{1,corr} = {} & \frac{A E_{xo}^{\gamma_1 - \gamma_2}}{\gamma_1 - 1} (E_1^{-\gamma_1 + 1} - E_{xo}^{-\gamma_1 + 1}) \\ & + \frac{A}{\gamma_2 - 1} (E_{xo}^{-\gamma_2 + 1} - E_{\max}^{-\gamma_2 + 1}), \end{aligned} \quad (10)$$

$$j_{2,corr} = \frac{A}{\gamma_2 - 1} (E_2^{-\gamma_2 + 1} - E_{\max}^{-\gamma_2 + 1}), \quad (11)$$

$$j_{3,corr} = \frac{A}{\gamma_2 - 1} (E_3^{-\gamma_2 + 1} - E_{\max}^{-\gamma_2 + 1}), \quad (12)$$

where E_1 = 30 keV, E_2 = 100 keV, and E_3 = 300 keV are the nominal energy thresholds of the three electron channels.

5. How the Corrections Affect the Electron Fluxes

[22] Let us next see how the corrections discussed above affect the electron fluxes. We corrected the electron fluxes

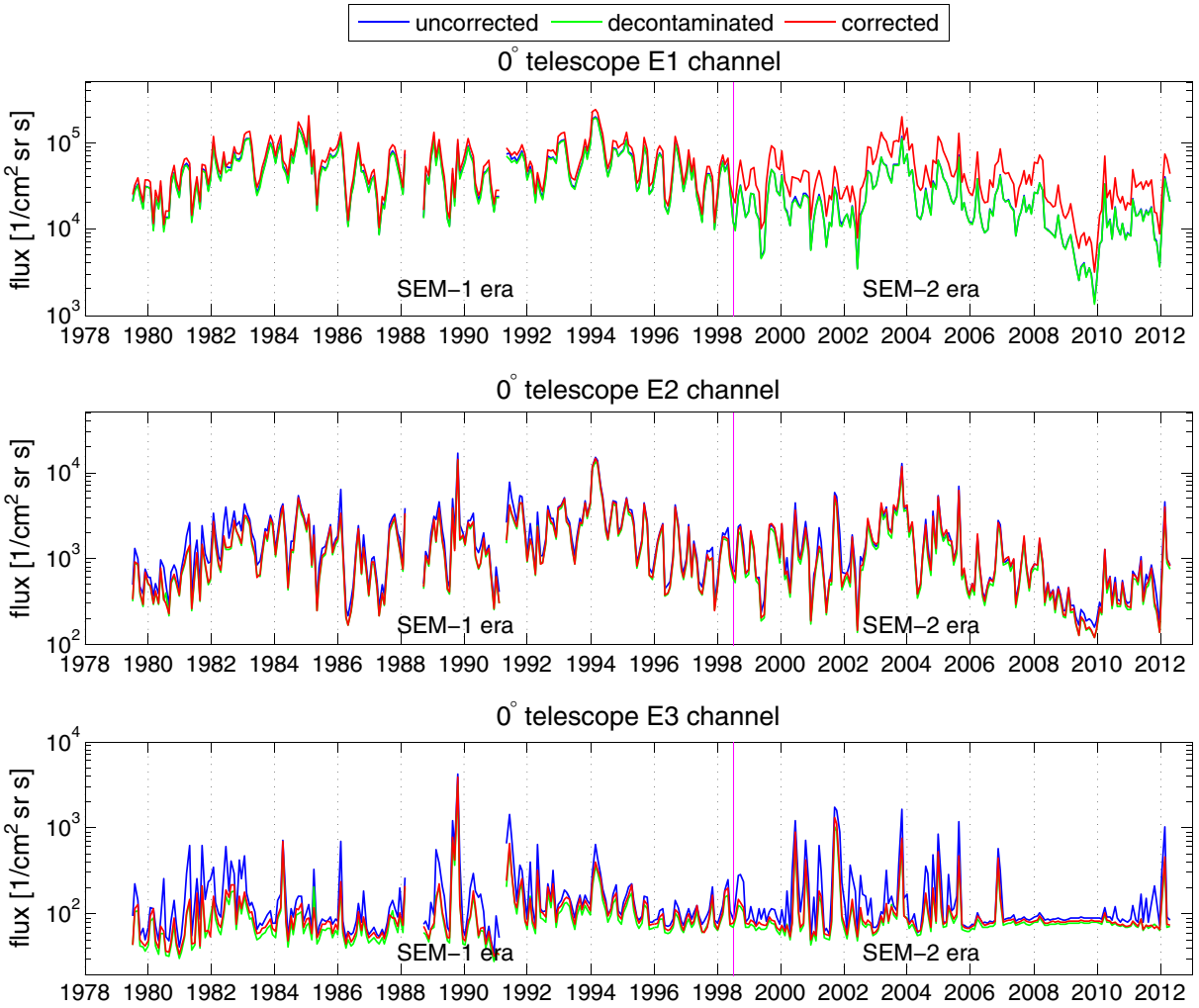

Figure 3. The 30 day averaged uncorrected (blue), decontaminated (green), and corrected (red) electron fluxes from the 0° telescope. The fluxes were computed from data of NOAA-06, NOAA-08, NOAA-10, NOAA-12, and NOAA-15 (which all have a similar dawn-dusk orbit) in the northern hemisphere above $L = 2$. Panels correspond to (top) E1, (middle) E2, and (bottom) E3 channels. The vertical pink line in mid-1998 denotes the change from SEM-1 to SEM-2.

of all NOAA satellites by applying the algorithms discussed above to the high resolution 16 s averaged measurements. To study the long-term evolution of the electron fluxes and the overall effect of correction, we computed 30 day averages of the fluxes, similarly as in *Asikainen et al.* [2012], from data of NOAA-06, NOAA-08, NOAA-10, NOAA-12, and NOAA-15 (which all have a similar dawn-dusk orbit) in the northern hemisphere above $L = 2$. The southern hemisphere and region $L < 2$ was excluded from this analysis because the correction of the data may be affected by the high fluxes of relativistic electrons in the South Atlantic Anomaly (relativistic electrons may cause contamination in certain energy channels of the proton instrument, which would in turn affect the removal of the proton contamination from the electron measurements). Figures 3 and 4 show these 30 day averaged electron fluxes for E1, E2, and E3 channels for 0° and 90° telescopes, respectively. The two figures show the uncorrected fluxes in blue, the decontaminated fluxes (i.e., corrected for proton contamination only) in green, and the corrected fluxes (i.e., after removing proton contamination and correcting for detector efficiency) in red. Figure 5 shows the ratios of the 30 day averaged corrected and uncorrected fluxes for the three energy channels for 0° (Figure 5a) and 90° telescopes (Figure 5b). For reference, the pink line in mid-1998 shown in Figures 3–5 separates the time series into SEM-1 and SEM-2 eras.

[23] Figure 3 shows that in E1 channel of the 0° telescope, the effect of correction is significant especially in SEM-2 instruments. As discussed above, the correction consists of two parts which affect the fluxes in opposite directions: removal of proton contamination decreases the fluxes, while the correction for detector efficiency increases them. In E1 channel, the net effect of the correction is to increase the fluxes, since the uncorrected and decontaminated fluxes are practically identical, indicating that the relative contribution of proton contamination to E1 channel is very small. This is because the electron fluxes at E1 channel typically far exceed the level of contaminating proton fluxes. For SEM-2 E1 channel, this increase is significantly larger than

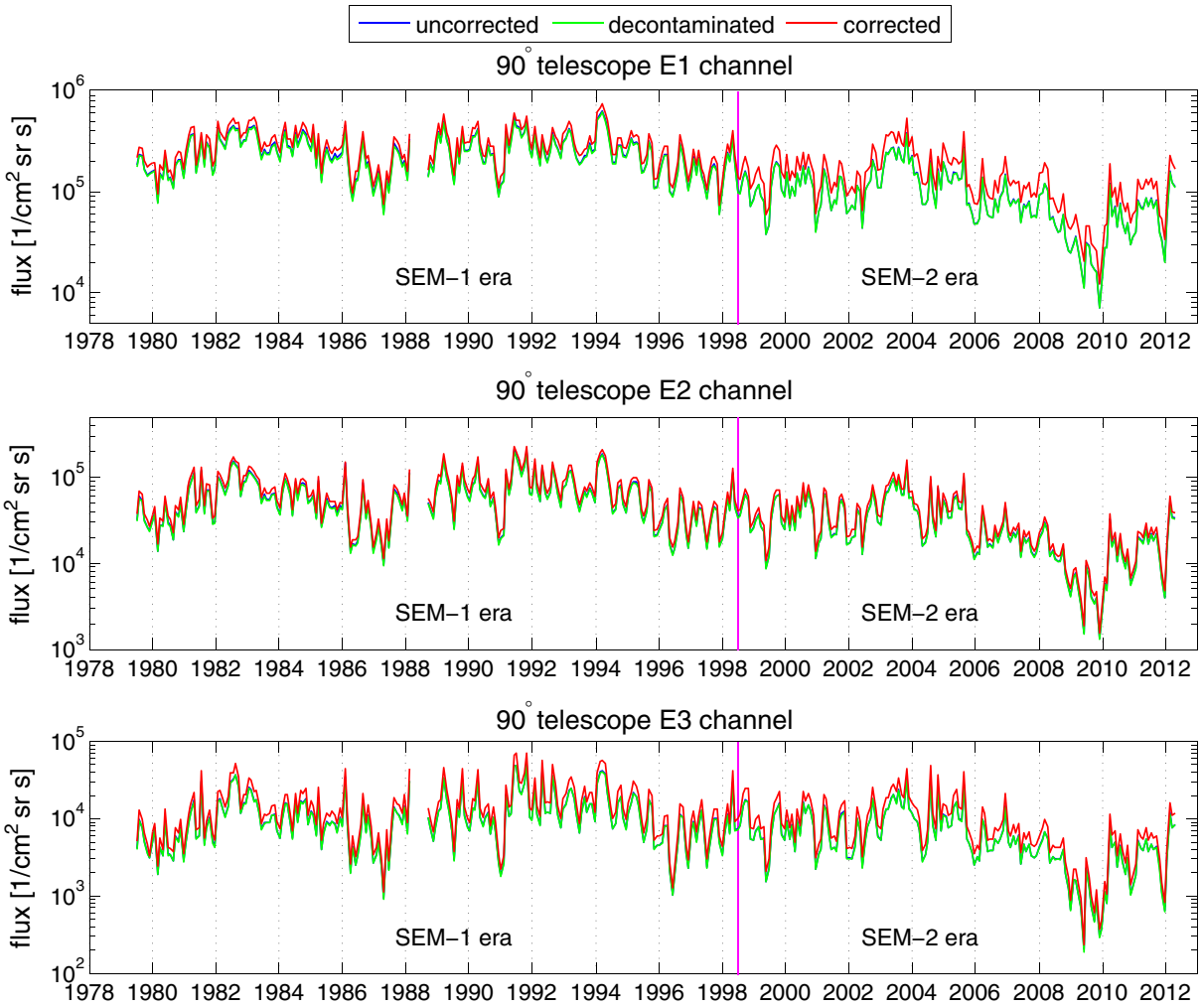

Figure 4. Same as Figure 3 for 90° telescope.

for SEM-1 E1. Figure 5a shows that, on an average, the correction raises SEM-1 E1 fluxes by a factor of 1.19 and SEM-2 E1 fluxes by a factor of 2.06. This difference is due to the significantly smaller efficiency of E1 channel in SEM-2 than in SEM-1, leading to a larger change in the flux in SEM-2 when correcting for the detector efficiency. One can see in Figure 3 that without the correction for detector efficiency, the long-term time series of E1 electron fluxes would be severely inhomogeneous due to the systematic difference between the SEM-1 and SEM-2 satellites even if the proton contamination was removed.

[24] In E2 channel of the 0° telescope, the net effect of correction is to reduce the fluxes slightly (see Figures 3 and 5a). In SEM-1 the corrected fluxes are quite close to the decontaminated fluxes indicating that the effect of detector efficiency is relatively smaller than the effect of proton contamination, because the detector efficiency is fairly close to the ideal. In SEM-2 the uncorrected, decontaminated, and corrected fluxes are all quite close to each other, because the thicker shielding is more effective in rejecting protons. However, in both SEM-1 and SEM-2, there are periods (e.g., 1980–1983, 1990–1992, and 2000–2002) when the difference between the corrected and uncorrected (and decontaminated) E2 fluxes is increased to be notable in Figure 3 (see also Figure 5a). These periods correspond to the early declining solar cycle phases when the proton fluxes are maximized (T. Asikainen and K. Mursula, Long-term evolution of corrected NOAA/MEPED energetic proton fluxes and their relation to geomagnetic indices, submitted to *Journal of Geophysical Research*, 2013). Overall, there is only a small systematic difference in the net effect of the correction between SEM-1 and SEM-2 E2 channels, which mainly results from the fact that SEM-1 is sensitive to protons of lower energies than SEM-2, making proton contamination slightly more severe in SEM-1. Figure 5a shows that in SEM-1, E2 fluxes are reduced on average by a factor of 0.84 and in SEM-2 by a factor of 0.94. Thus, the correction reduces the absolute level of the E2 fluxes slightly but, because of the small difference between these factors, the relative correction to the long-term homogeneity of fluxes is less than 12%.

[25] In E3 channel of the 0° telescope, the net effect of correction is to reduce the fluxes. Figure 3 shows that the decontaminated proton fluxes in both SEM-1 and SEM-2 are only slightly lower than the corrected fluxes. This indicates that, similarly as for the E2 channel, the difference between the uncorrected and corrected fluxes is mainly caused by proton contamination. As shown in Figure 5a in SEM-1, the

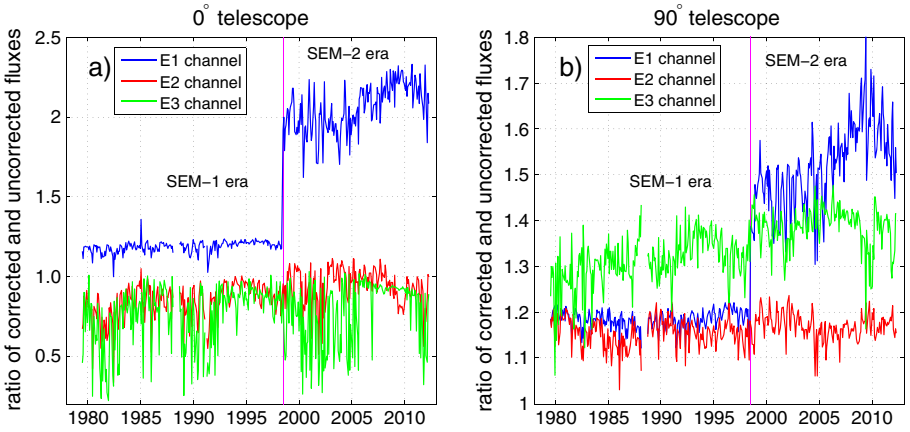

Figure 5. Ratios of 30 day averaged corrected and uncorrected fluxes in the three energy channels for (a) 0° telescope and (b) 90° telescope.

E3 fluxes are reduced on average by a factor of 0.76 and in SEM-2 by 0.78. However, momentarily, the reduction can be much larger, as is seen in Figures 3 and 5a. For example, in 1980–1983, the corrected monthly E3 fluxes are smaller than the uncorrected fluxes by a factor of 4. At these times the proton contamination in E3 channel dominates over the real electron fluxes. Note that the relative effect of proton contamination during these times is much larger in E3 than in E1 and E2 because the electron fluxes in E3 are much smaller than in the lower energy channels. The dominant contribution of contaminating protons in 0° E3 is seen most recently in the period of increasing activity in 2011, where the peaks of uncorrected electron fluxes (except for the final largest peak) are entirely due to proton contamination (see Figure 3). Note that the temporal development of 0° E3 fluxes seen in Figure 3 is very different from that of E1, E2, and even 90° E3 fluxes (see Figure 4), which display clear solar cycle related variation. The reason for this different behavior is the fact that the 0° E3 fluxes are often lower than the background noise level caused, e.g., by cosmic rays.

[26] Let us now discuss the effect of correction to the electrons of the 90° telescope depicted in Figures 4 and 5b. It is important to note that SEM-1 and SEM-2 90° fluxes are not directly comparable because the 90° detectors in SEM-1 and SEM-2 are roughly perpendicular to each other. Since SEM-1 90° telescope measures locally trapped particles all the time, while SEM-2 measures trapped particles at high latitudes and precipitating particles at low latitudes, the average SEM-1 90° fluxes are systematically larger. Note also that, at the satellite altitude, the pitch angle distribution of electrons is typically highly anisotropic, which is why the 90° fluxes are roughly an order of magnitude larger than the 0° fluxes (see also Figure 3). One can see that the relative effect of proton contamination is negligible in both the SEM-1 and SEM-2 90° telescopes in all three channels (uncorrected and decontaminated are nearly indistinguishable). As in the case of 0° E1 channel, this is because the electron fluxes in the 90° telescope are much larger than the contaminating proton fluxes. However, in all 90° channels, the corrected fluxes are clearly larger than the uncorrected fluxes, highlighting

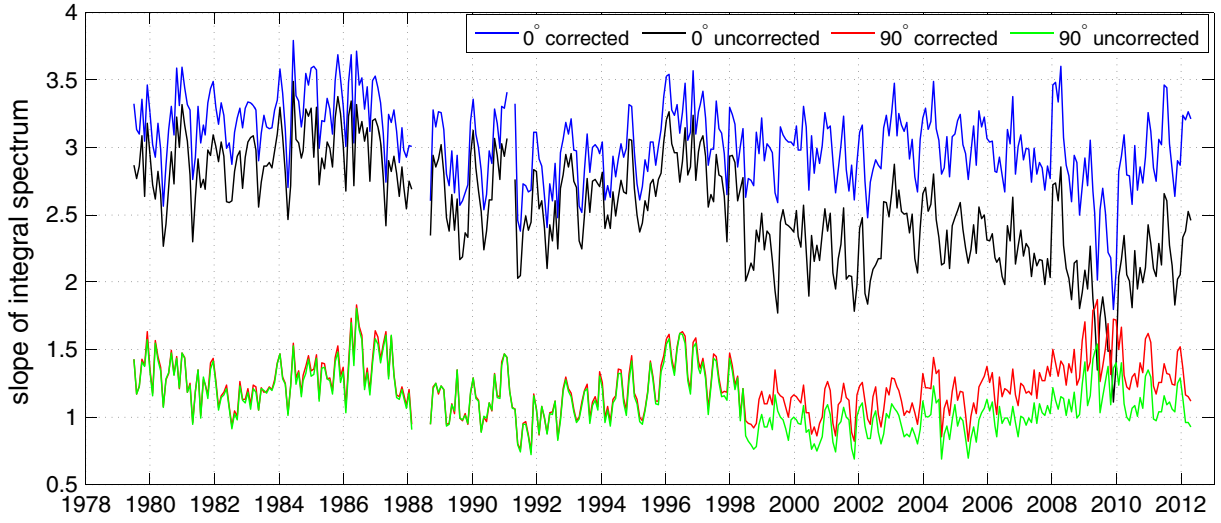

Figure 6. The 30 day averaged slope of the integral spectrum between 30 and 100 keV for the 0° and 90° telescopes. The blue and red curves correspond to the corrected 0° and 90° fluxes,respectively, while the black and green curves correspond to the uncorrected 0° and 90° fluxes, respectively. The slope of the integral spectrum is defined as $\log(j_{1,\mathrm{corr}}/j_{2,\mathrm{corr}})/\log(100/30)$.

the importance of the correction for detector efficiency. Figure 5b highlights the large systematic difference between SEM-1 and SEM-2 E1 channel caused by the very different detector efficiencies, similarly as for 0° telescopes. On an average, the 90° SEM-1 E1 fluxes are increased by a factor of 1.19 and SEM-2 E1 fluxes by a factor of 1.52. It is interesting to note that the factors for SEM-1 E1 are roughly equal for 0° and 90° telescopes, but for SEM-2 E1 channel the average factor for the 90° telescope is much smaller than for the 0° telescope (2.06). This difference is caused by a systematic difference between the electron spectra measured by the SEM-2 0° and 90° telescopes. Figure 6 shows the spectral slope between E1 and E2 channels defined as $\log(j_{1,\mathrm{corr}}/j_{2,\mathrm{corr}})/\log(100/30)$ (note that this is the slope of the integral spectrum and not the slope γ_1 of the differential spectrum defined above). One can see that the spectral slope is indeed systematically over two times larger in the 0° telescope than in the 90° telescope. Considering the detector efficiency of E1 channel (Figure 1) one can see that if we increase the spectral slope, the relative number of particles at those energies where the efficiency is small increases. Accordingly, for harder spectra (smaller spectral slopes) the ratio of corrected and uncorrected fluxes is expected to be smaller. Note that a similar difference in the 0° and 90° spectral slopes exists in SEM-1 also, but this leads to a much smaller difference in the corrected/uncorrected flux ratio between 0° and 90° than in SEM-2 because the efficiencies in SEM-1 E1 channel are generally significantly higher than in SEM-2 E1.

[27] Moving on to E2 channel of the 90° telescope, we see that the effect of the correction is dramatically different from that in the 0° telescope. The effect of proton contamination is negligible and the correction for detector efficiency increases the fluxes on average by a factor of 1.16 (1.17) in SEM-1 (SEM-2). Thus, the correction has an opposite effect for 90° fluxes to that for the 0° E2 fluxes. This is because the 90° fluxes are generally higher than the 0° fluxes, which makes the relative effect of proton contamination much smaller for the 90° telescope than for the 0° telescope where the proton contamination had a dominant effect. The effect of correction for the E3 channel in the 90° telescope is closely similar to E2 channel. The relative effect of proton contamination is negligible and the correction for detector efficiency increases the SEM-1 (SEM-2) fluxes on average by a factor of 1.31 (1.39).

[28] Figure 6 shows large differences between the corrected and uncorrected slopes in both 0° and 90° telescopes. The 0° slope is systematically almost three times larger than the 90° slope indicating that the precipitating electron spectrum is much softer than the trapped electron spectrum. The reason for this is likely because the lifetime of electrons in the loss cone is inversely proportional to their velocity (and thus energy). Thus, within the loss cone, electrons of higher energies are lost relatively faster than outside the loss cone when compared to the lower energy ones. Because of this difference in lifetimes, the trapped electron spectrum is harder than the precipitating spectrum. One can see from Figure 6 that for 0° telescope the change in the slope due to the correction is large for both SEM-1 and SEM-2, but for the 90° telescope, the change is only significant in SEM-2. These corrections to the spectral slope and the above discussed corrections to the absolute flux levels imply that the uncorrected MEPED electron fluxes greatly misrepresent the true form of the electron energy spectrum and the level of electron fluxes. This information is vitally important in many models and applications utilizing MEPED data, e.g., as a measure of energetic electron precipitation into the atmosphere [e.g., *Wissing and Kallenrode*, 2009; *Sinnhuber et al.*, 2011; *Andersson et al.*, 2012]. The present results will thus imply significant changes to many previous quantitative results based on MEPED electron data.

6. Conclusions

[29] In this work we have analyzed the electron detectors of the NOAA/MEPED instrument in great detail, considering two important effects which need to be corrected before the MEPED electron data can be reliably used. Using a 1-D numerical Monte Carlo simulation model, we estimated how the old (SEM-1) and new (SEM-2) versions of the electron detectors respond to incoming electrons and protons. The SEM-1 and SEM-2 electron instruments have some differences in their construction, the most significant being that the Ni foil shielding the instrument against incoming energetic protons is about 49% thicker in SEM-2. With the model simulation, we found that these differences have a dramatic effect on the detector efficiency not only for the contaminating protons but also for the electrons to be measured. The largest difference in detector efficiency between SEM-1 and SEM-2 is found for the E1 channel which nominally measures electrons above 30 keV. We showed that the detector response to electrons significantly deviates from an ideal step-like response for all energy channels, which calls for proper calibration of the measured fluxes. We also found that the detector response to contaminating protons, although in a fair agreement with the nominal, still deviates considerably from nominal and has to be corrected.

[30] Using the obtained results from the detector simulation, we developed a mathematical algorithm to correct the electron fluxes for proton contamination and nonideal detector efficiency. While removing the proton contamination reduces the electron fluxes, detector efficiency correction generally raises them. We showed that, on an average, in the 0° telescope, the correction for the detector efficiency has a large and dominant effect for the lowest energy E1 channel, but removing the proton contamination is more important for the E2 and E3 channels. In the 90° telescope, the electron fluxes in all energy channels are typically so high that proton contamination is usually negligible, and fluxes are slightly increased in all channels due to the detector efficiency correction. The corrected fluxes are in many cases significantly different from the uncorrected fluxes. The largest correction is found for the E1 channel of the SEM-2 0° telescope, where the corrected fluxes are, on an average, more than two times larger than the uncorrected fluxes. The most important outcome of the correction is that it removes the inhomogeneity in the MEPED electron measurements due to the differences between SEM-1 and SEM-2 detectors. Without the correction, the long-term evolution of electron fluxes would be significantly misrepresented.

[31] Since the correction changes the different energy channels differently, it also changes the form of the electron spectrum. We showed that the spectral slopes are dramatically altered by correction, especially for the 0° telescope (average SEM-2 slope changed from 2.2 to 3.0). Generally,

the corrected electron spectra are softer than the uncorrected ones, which indicates that the relative amount of lower energy electrons is underestimated in the uncorrected data. When considering the effect of electron precipitation (described mainly by electron fluxes of the 0° telescope) on atmospheric ionization profiles and production of various ion species (e.g., NOx and HOx), an accurate knowledge of the electron energy spectrum is extremely important. The work presented here provides currently the longest calibrated series of direct energetic electron measurements in space physics, and will allow more accurate studies of, e.g., the atmospheric response to electron precipitation during several solar cycles.

[32] **Acknowledgments.** We acknowledge the discussions with Dave Evans and Janet Green on analyzing the MEPED instruments and data. We acknowledge the support by the Academy of Finland to projects 257403, 264994, and 128189. We gratefully acknowledge support for this work via the Near-Earth Space Data Infrastructure for e-Science project (www.espas-fp7.eu), which is funded by the Research Infrastructures theme of the EU Framework 7 programme under grant agreement 283676.

[33] Masaki Fujimoto thanks the reviewers for their assistance in evaluating this paper.

References

Andersson, M., P. T. Verronen, S. Wang, C. J. Rodger, M. A. Clilverd, and B. R. Carson (2012), Precipitating radiation belt electrons and enhancements of mesospheric hydroxyl during 2004–2009, *J. Geophys. Res.*, *117*, D09304, doi:10.1029/2011JD017246.

Asikainen, T., and K. Mursula (2011), Recalibration of NOAA/MEPED energetic proton measurements, *J. Atmos. Solar-Terrestrial Phys.*, *73*, 335–347, doi:10.1016/j.jastp.2009.12.011.

Asikainen, T., K. Mursula, and V. Maliniemi (2012), Correction of detector noise and recalibration of NOAA/MEPED energetic proton fluxes, *J. Geophys. Res.*, *117*, A09204, doi:10.1029/2012JA017593.

Callis, L. (2005), Odd nitrogen formed by energetic electron precipitation as calculated from TIROS data, *Geophys. Res. Lett.*, *24*(24), 3237–3240, doi:10.1029/97GL03276.

Codrescu, M., and I. Fuller-Rowell (1997), Medium energy particle precipitation influences on the mesosphere and lower thermosphere, *J. Geophys. Res.*, *102*(A9), 19,977–19,987.

Elad, E., C. Inskeep, R. Sareen, and P. Nestor (1973), Dead layers in charged-particle detectors, *IEEE Trans. Nucl. Sci.*, *20*, 534–544.

Evans, D. S., and M. S. Greer (2000), Polar orbiting environmental satellite space environment monitor—2: Instrument descriptions and archive data documentation, *NOAA Technical Memorandum, OAR SEC-93*, Space Environment Center, Boulder, Colo.

Galand, M., and D. Evans (2000), Radiation damage of the proton MEPED detector on POES (TIROS/NOAA) satellites, *NOAA Technical Memorandum, OAR 456-SEC 42*, U.S. Department Of Commerce, National Oceanic and Atmospheric Administration, Space Environment Center, Boulder, Colo.

Hill, V. J., D. S. Evans, and H. H. Sauer (1985), TIROS-N/NOAA satellites Space Environment Monitor archive tape documentation, *NOAA Technical Memorandum, ERL SEL-71*, U.S. Dept. of Commerce, National Oceanic and Atmospheric Administration, Environmental Research Laboratories, Boulder, Colo.

Lam, M., R. Horne, N. Meredith, S. Glauert, T. Moffat-Griffin, and J. Green (2010), Origin of energetic electron precipitation > 30 keV into the atmosphere, *J. Geophys. Res.*, *115*, A00F08, doi:10.1029/2009JA014619.

McFadden, J., et al. (2007), In-flight instrument calibration and performance verification, in *Calibration of Particle Instruments in Space Physics, ISSI Scientific Report,* vol. SR-007, edited by M. Wüest, D. S. Evans, and R. von Steiger, pp. 277–385, ESA Publications Division, Noordwijk, The Netherlands.

Raben, V. J., D. S. Evans, H. H. Sauer, S. R. Sahm, and M. Huynh (1995), TIROS/NOAA satellite Space Environment Monitor data archive documentation: 1995 update, *NOAA Technical Memorandum, ERL SEL-86*, Space Environment Laboratory, Boulder, Colo.

Rodger, C., M. Clilverd, J. Green, and M. Lam (2010), Use of POES SEM-2 observations to examine radiation belt dynamics and energetic electron precipitation into the atmosphere, *J. Geophys. Res.*, *115*, A04202, doi:10.1029/2008JA014023.

Rozanov, E., L. Callis, M. Schlesinger, F. Yang, N. Andronova, and V. Zubov (2005), Atmospheric response to NOy source due to energetic electron precipitation, *Geophys. Res. Lett.*, *32*, L14811, doi:10.1029/2005GL023041.

Seale, R. A., and R. H. Bushnell (1987), The TIROS-N/NOAA A-J Space Environment Monitor subsystem, National Oceanic and Atmospheric Administration, Boulder, Colo., NOAA Technical Memorandum, ERL SEL-75.

Sinnhuber, M., S. Kazeminejad, and J. M. Wissing (2011), Interannual variation of NOx from the lower thermosphere to the upper stratosphere in the years 1991–2005, *J. Geophys. Res.*, *116*, A02312, doi:10.1029/2010JA015825.

Truscott, P., et al. (2003), MULASSIS—Monte Carlo radiation shielding simulation for space applications made easy, in *RADECS 2003: Proceedings of the 7th European Conference on Radiation and Its Effects on Components and Systems*, edited by K. Fletcher, pp. 191–196, European Space Agency, Noordwijk, The Netherlands.

Wissing, J. M., and M.-B. Kallenrode (2009), Atmospheric Ionization Module Osnabruck (AIMOS): A 3-D model to determine atmospheric ionization by energetic charged particles from different populations, *J. Geophys. Res.*, *114*, A06104, doi:10.1029/2008JA013884.

Yando, K., R. Millan, J. Green, and D. Evans (2011), A Monte Carlo simulation of the NOAA POES medium energy proton and electron detector instrument, *J. Geophys. Res.*, *116*, A10231, doi:10.1029/2011JA016671.